Cloud-Property Retrievals from Off-Beam/Multiple-Scattering Lidar Data Collected in Space and from Ground

ANTHONY B. DAVIS, STEVEN P. LOVE AND CHENG HO

Los Alamos National Laboratory, Space & Remote Sensing Sciences Group (NIS-2), Los Alamos, NM 87545, USA

DAVID M. WINKER AND MARK VAUGHAN

NASA's Langley Research Center, Atmospheric Sciences Division (MS 475), Hampton, Va 23681, USA

ROBERT F. CAHALAN

NASA's Goddard Space Flight Center, Climate & Radiation Branch (Code 913), Greenbelt, Md 20771, USA

ABSTRACT

Cloud lidar data from NASA's Lidar-In-space Technology Experiment (LITE) mission and from LANL's new Wide-Angle Imaging Lidar (WAIL) prototype are used to show that the multiple-scattering theory of off-beam lidar can readily explain the observations, conditional that internal stratification of cloud density is accounted for. At the same time, predictions for spatial and temporal statistics of the signals are used to infer the optical depth and physical thickness of the clouds being probed.

1. Introduction and Outline

In most standard —indeed, "on-beam"— atmospheric applications of light radar, the data is interpreted with the so-called lidar equation, actually the radar equation with the added effects of two-way extinction; this well-known formula is based on a single-scattering approximation to the time-dependent radiative transfer equation (RTE). By contrast, in "off-beam" lidar multiply-scattered photons dominate the signal, so the data is interpreted with the so-called Green function (GF) for the time-dependent RTE; this is a special solution of the RTE for a source which is a Dirac δ-function in space, time, and direction that models the pulsed laser beam. There is no analytical theory for the space-time GF for optical media of finite thickness, even if they are homogeneous; we therefore use the photon diffusion approximation to guide our analysis of the information content of off-beam lidar signals. This analysis shows that the most robust components of the off-beam signal are determined by the physical thickness and optical depth of the cloud. In this report, we show that very reasonable estimates for cloud properties can be inferred when off-beam lidar theory is applied to real cloud data collected in space and from ground.

In the following section, we survey the elements of off-beam cloud lidar theory required for this study. In section 3, we confront theoretical time-domain predictions with data collected during NASA's Lidar-In-space Technology Experiment (LITE) mission as the Space Shuttle was overlying marine stratocumulus (Sc). In section 4, we present, analyze and interpret newly acquired space-time data from ground level with the prototype Wide-Angle Imaging Lidar (WAIL) system assembled at LANL/NIS-2. We draw conclusions from the encouraging results in both configurations and describe future work in section 5.

2. Off-Beam Cloud Lidar Theory

a. Definitions

The schematic in Fig. 1 describes the geometry of off-beam cloud lidar observations. The key quantities are cloud optical depth (τ), physical thickness (Δ_z), asymmetry factor of scattering phase function (g), and range (δ_{obs}). The remotely observable radiative transfer GFs for a δ-source at the cloud boundary (G_{obs}) will depend parameterically on all of these cloud quantities as well as two independent variables for space and one for time. The spatial variable can be determined in Cartesian coordinates (x,y) measured away from the point-source, cylindrical coordinates (ρ,φ) convenient when the detector is at very large range ($\delta_{obs} >> \Delta_z$), or else polar angles (θ_ρ,φ) when the cloud is at relatively close range (then $\tan\theta_\rho = \rho/\delta_{obs}$). The temporal variable can be either time elapsed since the pulse impacted the cloud (t), or the "in-cloud" pathlength ($\lambda = ct$), noting that the "out-of-cloud" pathlength is simply $\delta_{obs}(1+1/\cos\theta_\rho)$. The instrumental parameters that affect non-trivially the observed signal are laser-beam diameter and pulse width for the transmitter (smoothing of space-time GF), as well as the field-of-view (FOV) of the receiver optics (spatial truncation of the GF).

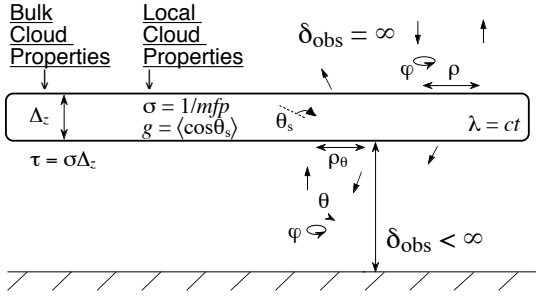

FIG. 1. *Geometry of Off-Beam Cloud Lidar*. From left to right, illustrated meanings for: (1) cloud optical depth τ, physical thickness Δ_z, their ratio (extinction σ), and asymmetry factor g (mean cosine of scattering angle ≈ 0.85 for typical droplet populations); (2) independent variables angle (space) θ_ρ and time t, radiance $G_{obs}(\tau,g,\Delta_z,\delta_{obs};t,\theta_\rho,\varphi)$ for a ground-based WAIL system and a cloud at finite range δ_{obs}; (3) similarly, $G_{obs}(\tau,g,\Delta_z,\infty;t,\rho,\varphi)$ is measured during a LITE-like mission in space and has been extensively studied elsewhere (Winker 1997; Miller and Stephens, 1999).

Photon-escape GFs have straightforward interpretations in terms of probability of a photon to escape from the

cloud into any direction at position (x,y) and time t, conditional to be either reflected or transmitted: e.g.,

$$G_R(t,x,y)\mathrm{d}x\mathrm{d}y\mathrm{d}t \,/\, R = \mathrm{Prob}\{\text{ escape during } [t,t+\mathrm{d}t), \text{ from } [x,x+\mathrm{d}x)\otimes[y,y+\mathrm{d}y) \mid \text{ in reflection }\}, \quad (1)$$

where the normalization constant,

$$R = \iiint G_R(t,x,y)\mathrm{d}x\mathrm{d}y\mathrm{d}t, \quad (2)$$

is simply cloud albedo for normal incidence. Analogous relations can be written for transmission where, by conservation at most lidar wavelengths, we have $T = 1-R$. Normalized escape GFs can thus be treated as probability density functions and we can compute their moments.

If detailed information about the space/time-dependent bi-directional properties of the cloud's radiative GFs is not available, then we make a standard Lambertian hypothesis:

$$G_R(t,x,y)\mathrm{d}x\mathrm{d}y\mathrm{d}t \approx \pi G_{obs}(t,\theta_\rho,\varphi)\sin\theta_\rho \mathrm{d}\theta_\rho \mathrm{d}\varphi \mathrm{d}t. \quad (3)$$

As shown in the following, the l.h. side can be computed analytically in diffusion theory while the r.h. side requires a numerical approach such as Monte Carlo (MC) to avoid the Lambertian assumption.

b. Low-Order Statistical Moments of Radiative GFs

The simplest in-cloud propagation characteristics of a laser pulse are: mean photon pathlength,

$$\langle\lambda\rangle_R = c\langle t\rangle_R = c\iint \mathrm{d}x\mathrm{d}y\left[\int t G_R(t,x,y)\mathrm{d}t\right] / R; \quad (4)$$

its 2nd-order moment (used in path variance $\langle\lambda^2\rangle_R - \langle\lambda\rangle_R^2$),

$$\langle\lambda^2\rangle_R = c^2\langle t^2\rangle_R = c^2\iint \mathrm{d}x\mathrm{d}y\left[\int t^2 G_R(t,x,y)\mathrm{d}t\right] / R; \quad (5)$$

root-mean-square (rms) horizontal transport $\sqrt{\langle\rho^2\rangle_R}$, where

$$\langle\rho^2\rangle_R = \int \mathrm{d}t\left[\iint (x^2+y^2) G_R(t,x,y)\mathrm{d}x\mathrm{d}y\right] / R \quad (6)$$

which is also the variance of ρ since $\langle x\rangle_R = \langle y\rangle_R = 0$, by symmetry. One can also think of $\langle\rho^2\rangle_R^{1/2}$ as the gyration radius of the spot of diffuse light excited by the laser in cw mode. There are of course analogous quantities for transmission (subscript "T") that have been used in other studies, cf. Savigny et al. (1999).

A major advantage of using the observables in Eqs. (4–6) is that there is no need for absolute calibration to estimate them from observations using Eqs. (1–3).

c. Photon Diffusion Predictions for Radiative GFs

In absence of absorption, only two scales are required to determine the optical properties of a plane-parallel slab: the outer-scale Δ_z, and the inner-scale defined by the photon mean-free-path (MFP), $l = 1/\sigma = \Delta_z/\tau$. In the diffusion approximation, we are more interested in the "transport" MFP

$$l_t = l/(1-g) = 1/[(1-g)\sigma] \quad (7)$$

which is in essence the MFP for an effectively isotropic scattering; the rescaling by $(1-g)^{-1} \approx 6.7$ takes care of the propensity for forward scattering. One final parameter is introduced in diffusion theory to describe boundary conditions: the "extrapolation length" which we will denote χl_t. Here χ is an $O(1)$ numerical factor that can be used to minimize the approximation error.

A spatial-Fourier/temporal-Laplace solution of the non-stationary three-dimensional diffusion equation by Davis et al. (1999) with boundary/initial conditions describing a pulsed point-source leads to:

$$R = \frac{\Delta_z}{\Delta_z + 2\chi l_t} = \frac{(1-g)\tau}{(1-g)\tau + 2\chi} \quad (8)$$

for albedo in Eq. (2);

$$\langle\lambda\rangle_R = 2\chi \times \Delta_z \times \left[\,1 + C\left(\frac{\chi}{(1-g)\tau}\right)\,\right] \quad (9)$$

for mean pathlength in Eq. (4); and

$$\langle\lambda^2\rangle_R = \frac{4\chi}{5} \times \Delta_z^2 (1-g)\tau \times \left[\,1 + C'\left(\frac{\chi}{(1-g)\tau}\right)\,\right] \quad (10)$$

for the 2nd moment of pathlength in Eq. (5); and

$$\langle\rho^2\rangle_R = \frac{8\chi}{3} \times \frac{\Delta_z^2}{(1-g)\tau} \times \left[\,1 + C''\left(\frac{\chi}{(1-g)\tau}\right)\,\right] \quad (11)$$

for the variance in horizontal transport defined in Eq. (6). The radiative quantities in (9–11) contain pre-asymptotic correction terms given by:

$$C(\varepsilon) = C''(\varepsilon) = \varepsilon(1+3\varepsilon)/(1+2\varepsilon), \quad (12a)$$

$$C'(\varepsilon) = \varepsilon(8+41\varepsilon+75\varepsilon^2+\varepsilon^3)/(1+2\varepsilon)^2; \quad (12b)$$

these corrections become small as

$$1/\varepsilon = (1-g)\tau/\chi = \Delta_z/(\chi l_t) \quad (13)$$

increases. Figure 2 shows $T = 1-R$, $\langle\lambda\rangle_R$, $\langle\lambda^2\rangle_R^{1/2}$, and $\langle\rho^2\rangle_R^{1/2}$ from Eqs. (8–13) with $\Delta_z = 1$ and $\chi = 0.57$ as well as from straightforward MC simulations in units.

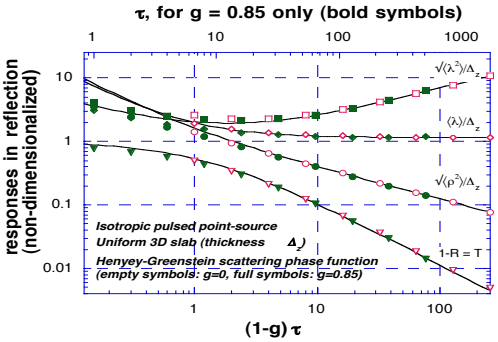

FIG. 2. *Analytical and Numerical Results for Off-Beam Cloud Lidar Observables*. From bottom to top, we have plotted $1-R$, $\langle\rho^2\rangle_R^{1/2}$, $\langle\lambda\rangle_R$, and $\langle\lambda^2\rangle_R^{1/2}$, from Eqs. (8–13) with $\chi = 0.57$. MC results are also plotted for isotropic and forward scattering phase functions (Henyey-Greenstein model with $g = 0.85$). We note the good collapse of the numerical results when they are plotted against $(1-g)\tau$. Agreement with the analytical diffusion results is excellent in the asymptotic ($\tau \geq 10$) .regime and reasonably good in the pre-asymptotic ($1 < \tau < 10$) region with the correction terms in Eqs. (12a,b).

Representative cloud parameters for a stratus layer are $g = 0.85$, τ in the range 7–70, hence $1 \leq (1-g)\tau \leq 10$, with Δ_z in the corresponding range 300–500 m. Using these values in Fig. 2 leads to an albedo R between 0.5 and 0.1, an rms "spot-size" $\langle\rho^2\rangle_R^{1/2}$ around 300 m, $\langle\lambda\rangle_R \approx$ 500–600 m, and the ratio $\langle\lambda^2\rangle_R^{1/2}/\langle\lambda\rangle_R$ falls between 1.5 and 2.

Finally, we note that, apart from exact proportionality constants, the leading terms in (8–10) can be obtained from simpler arguments based on the fractal properties of the random walks of the photons in the finite slab that defines the cloud (Davis et al., 1997; Davis, 1999).

3. Cloud Properties from LITE Data Analysis

The leading terms in Eqs. (8–11) from the diffusion-based and numerically-validated theory presented in the previous section suggest that any two of these four observables can be used to infer τ and Δ_z, given that g varies little in real clouds. Note that using albedo R alone from Eqs. (2) and (8), i.e., with no spatial or temporal information, can yield only the dimensionless optical depth τ. This is in fact the basic strategy in passive cloud remote sensing in the solar spectrum. However, proper measurement of R calls for an absolute calibration of the passive or active device. We therefore prefer to work with the remaining quantities.

The possibility of using only the two purely temporal quantities defined in Eqs. (4–5) and estimated in the associated diffusion Eqs. (8–9) is particularly interesting for off-beam lidar systems in low-Earth orbit where it is difficult at best to obtain the radial information used in Eq. (6). We are dealing here the first two moments of the returned pulse shape, independent of exit position.

This remote-sensing strategy can be tested directly with pulse shapes obtained during the shuttle-based LITE mission (Winker et al., 1996) for the marine Sc case-study. This occurred during the night-side of orbit 135 when the large FOV of 3.5 10^{-3} rad was used in conjunction with the low-gain setting to avoid saturation effects resulting from such reflective targets. From the 260 km orbit, this FOV gives a foot-print of 910 m for a beam diameter of 280 m. So ρ is sampled by LITE between 0 and 600 m $\approx$ 2 rms spot-radii from our above estimates based on Eq. (11) and Fig. 2. In this spatial sense, LITE and future space-borne lidar systems are "off-beam;" we will see that, in ground-based and airborne systems with clouds at close range, the same expression has an angular meaning too.

At any rate, we can expect to see very high orders-of-scattering in LITE signals: mean pathlengths $\langle\lambda\rangle_R$ should be $\approx$500–600 m, and rms pathlengths $\langle\lambda^2\rangle_R^{1/2}$ up to twice that much. In particular, this brings in pulse shapes with relatively long multiple-scattering tails; in terms of echo range (cloud-top altitude – 2 × extreme pathlength), this means that apparent echoes coming from negative altitudes are very likely.

Figure 3a shows two typical non-saturated 532 nm pulse profiles recorded during LITE as a function of both in-cloud pathlength and apparent echo altitude, using the available range information. The multiple-scattering pulse tail is highlighted and the anticipated echoes from below sea level are indeed observed. We must however caution ourselves about predictions based on a cloud model that is assumed homogeneous, vertically as well as horizontally. Horizontal structure is largely smoothed in foot-prints in the range 0.5 to 1 km (Marshak et al., 1995), at least in marine Sc. In sharp contrast, the time-domain signals will be affected by the persistent vertical gradients in liquid water content (LWC), hence in extinction

$$\sigma(z) = \frac{3LWC(z)}{2\rho_w r_e(z)} \tag{14}$$

where r_e is effective droplet radius and ρ_w is water density.

We have therefore numerically re-evaluated the radiative quantities in Eqs. (4–6) for cloud models with variable τ that are stratified with a linear increase in $\sigma(z)$ starting at 0 from cloud-base. Figure 3b shows the revised theoretical curves for $\langle\lambda^2\rangle_R^{1/2}/\langle\lambda\rangle_R$ (lower curve and l.h. vertical axis) and $\Delta_z/\langle\lambda\rangle_R$ (upper curve and readings on the r.h. vertical axis). Noting that the latter is the inverse of $\langle\lambda\rangle_R/\Delta_z$ in Fig. 2, we see that the new time-domain results (symbols) are systematically smaller that in the homogeneous-cloud case, as expected because the cloud is denser (smaller MFP) in the upper layers that are preferentially probed by the LITE system.

The data in Fig. 3a along with two intermediate pulses is also used in Fig 3b in a 2-step cloud-property retrieval scheme. First, the observed $\langle\lambda^2\rangle_R^{1/2}/\langle\lambda\rangle_R$ ratio of 1.38 is used to find a plausible range for the optical depth τ, cf. two intercepts and readings on the horizontal axis. Given the uncertainties in the data and in the theory, "plausible range" is a far better description of the situation than "a choice of two possible values." Then this range in τ is used in conjunction with $\langle\lambda\rangle_R \approx 515$ m to infer a range for Δ_z, noting that the higher value of 11 for τ makes more sense than the low value of 1.5 under the present circumstances. However, the inferred range for Δ_z is quite narrow anyway. In summary, the data and modeling is consistent with $\tau \approx 10$ and $\Delta_z \approx 380$ m. Both values are quite reasonable for a nocturnal marine boundary-layer Sc deck.

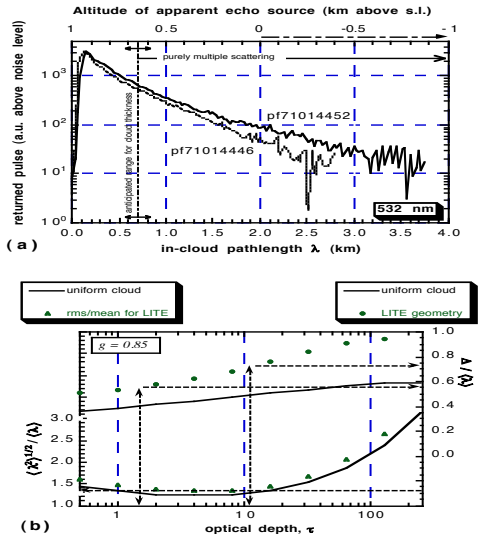

FIG. 3. *LITE Pulses from Marine Sc and Inferred Cloud Properties*. (a) Two unsaturated pulses returned at 532 nm. (b) The average of 4 pulses is used to estimate the cloud parameters from $\langle\lambda^q\rangle_R$, q = 1,2: $\tau \approx 10$, $\Delta_z \approx 380$ m (see text).

4. Cloud Properties from WAIL Data Analysis

The WAIL (Wide-Angle Imaging Lidar) concept comes from the idea of off-beam/multiple-scattering cloud lidar from close range. Indeed, referring to the ground-based configuration in Fig. 1, the outer parts of the diffuse spot are found at a zenith viewing angle

$$\theta_{2\rho_{rms}} = \tan^{-1}[2\sqrt{\langle\rho^2\rangle}_R/\delta_{obs}] \tag{15}$$

corresponding to twice the rms spot radii. For the typical cloud parameters used previously and $\delta_{obs} \approx 1$ km, this leads to $\theta_{2\rho_{rms}} \approx 30°$. So the expression "off-beam" lidar has here an angular as well as a spatial connotation.

Three of the present authors have reported on laboratory experiments in off-beam lidar scaled-down by a factor $\approx$1000÷1 (Davis, Ho, and Love, 1998). They used the original Remote Ultra-Low Light Imaging (RULLI) system described by Priedhorsky et al. (1996) as a receiver with a pathlength resolution of $\approx$3 cm and a 4.6° FOV at the focal plane of an f/5 Matsukov telescope with a 10 cm aperture; the sensitivity is such that an eye-safe (7 μW, 1.6 MHz) diode laser transmitter is sufficient. It was aimed at a surrogate cloud in a 0.88×0.66×0.44 m^3 aquar-

ium (the last dimension being Δ_z) filled with a highly scattering material at about 7.5 m range.

The WAIL group at LANL/NIS-2 has since modified the RULLI system to bin pathlength in 13.3 m intervals; its optics were replaced by a standard f/3.5–16 SLR 35-mm lens with a 60° FOV. The transmitter is now a doubled Nd:YAG laser that delivers 5 W at a 12 KHz rep-rate. After this re-configuration, the WAIL system was fielded on two occasions in 1999. Once the prescribed exposure time has elapsed, WAIL photon counts are reprocessed into 256×256×2048 data-cubes which are in turn used to compute the radiative quantities in Eqs. (4–6) after obtaining the cloud range δ_{obs}.

Before interpreting the WAIL field results with off-beam lidar theory, we need to make the same remark as for LITE: clouds are generally stratified and, this time, we are probing them from below where the extinction is lower (MFP is larger) than average. Figures 4a–b show ratios $\Delta_z/\langle\lambda\rangle_R$, $\langle\lambda^2\rangle_R^{1/2}/\langle\lambda\rangle_R$, and $\langle\rho^2\rangle_R^{1/2}/\langle\lambda\rangle_R$ as functions of τ for clouds with a linear increase in extinction σ with z for WAIL (bold symbols), a linear decrease in σ with z for LITE (empty symbols) for reference, and σ uniform in z also for reference (solid lines). As expected, the space- and time-scales are systematically larger here than in the uniform extinction case; however, the ratio of rms spot radius to mean pathlength changes little for both WAIL and LITE geometries.

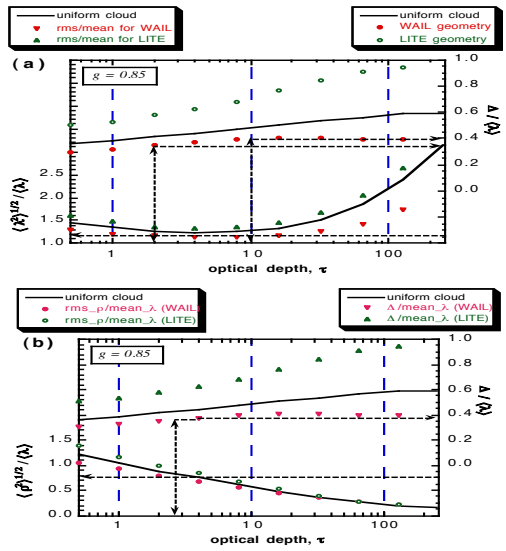

FIG. 4. *Inference of Cloud Properties from WAIL Data*. For examples of WAIL space-time "movies," consult web-page at <http://nis-www.lanl.gov/~love/clouds.html>. (a) Time-only scheme similar to Fig. 3b for LITE data. (b) Space-time scheme yielding similar results as in panel (a). See main text.

Data-cubes for the densest cloud observed during the second field experiment yield $\delta_{obs} \approx 2.5$ km, $\langle\lambda\rangle_R \approx 1.37$ km, $\langle\lambda^2\rangle_R^{1/2}/\langle\lambda\rangle_R \approx 1.16$, and $\langle\rho^2\rangle_R^{1/2}/\langle\lambda\rangle_R \approx 0.78$. These data are used in Fig. 4a exactly as LITE data was used in Fig. 3b. In Fig. 4b, the $\langle\rho^2\rangle_R^{1/2}/\langle\lambda\rangle_R$ ratio is instead of $\langle\lambda^2\rangle_R^{1/2}/\langle\lambda\rangle_R$ in Fig. 4a. The time-only scheme used in Fig. 4a leads to $2 \le \tau \le 10$ and 0.48 km $\le \Delta_z \le$ 0.55 km while the space-time scheme yields $\tau \approx 2.6$ and $\Delta_z \approx 0.52$ km. We have no standard of comparison here but these results are quite reasonable for a mid-level cloud. The consistency between the two approaches is however the most encouraging outcome of this exercise. In particular, we note that, without using the theoretical curve with the appropriate gradient in σ, the observed $\langle\lambda^2\rangle_R^{1/2}/\langle\lambda\rangle_R$ ratio of ≈1.16 would appear as unachievable.

5. Conclusions & Outlook

We have shown that "off-beam" lidar signals from clouds dominated by multiply-scattered photons collected in space during LITE and from ground using a prototype WAIL system can be used to infer such basic cloud properties as physical thickness and optical depth. Although the outcome of these retrievals can not be verified by independent means at this point in time, they are (1) internally consistent with each other when more than two observables are used, and (2) consistent with what we know of the cloud systems being probed.

The next steps are, on the one hand, to scrutinize the LITE archive for collocated air-truth data and, on the other hand, to set up the WAIL prototype near other cloud probing devices (mm-radar, microwave radiometers, radiosondes, etc.) in order to compare results. WAIL is presently limited to night-time operation but we are investigating new sources and filters to give it day-time capability and, therefore, to capture the full diurnal cycle.

REFERENCES

Davis, A.B., D.M. Winker, A. Marshak, J.D. Spinhirne, R.F. Cahalan, S.P. Love, S.H. Melfi, and W.J. Wiscombe, 1997: Retrieval of physical and optical cloud thicknesses from space-borne and wide-angle lidar, *Advances in Atmospheric Remote Sensing with Lidar*, Eds. A. Ansmann et al., Springer-Verlag, pp. 193–196.

Davis, A.B., C. Ho, and S.P. Love, 1998: Off-Beam (Multiply-Scattered) Lidar Returns from Stratus, 2: Space-Time Measurements in a Laboratory Simulation, *19th International Laser Radar Conference Proceedings*, Eds. U. Singh et al., pp. 55–58, July 6–10, 1998, Annapolis (Md), NASA Center for Aero-Space Information (CASI).

Davis, A.B., R.F. Cahalan, J.D. Spinhirne, M.J. McGill, and S.P. Love, 1999: Off-beam lidar: An emerging technique in cloud remote sensing based on radiative Green-function theory in the diffusion domain, *Phys. Chem. Earth (B)*, **24**, 757–765.

Davis, A.B., 1999: Physical thickness and optical depth of stratocumulus from space-borne lidar, A moment-based diffusion method, *Technical Digest of OSA Topical Meeting on "Optical Remote Sensing of the Atmosphere"*, pp. 66–68, June 21–25, 1999, Santa Barbara (Ca), Optical Society of America, Washington (DC).

Marshak, A., A.B. Davis, W.J. Wiscombe, and R.F. Cahalan, 1995: Radiative smoothing in fractal clouds, *J. Geophys. Res.*, **100**, 26247–26261.

Miller, S.D., and G.L. Stephens, 1999: Multiple scattering effects in the lidar pulse stretching problem, *J. Geophys. Res*, **104**, 22205–22219.

Priedhorsky, W.C., R.C. Smith, and C. Ho, 1996: Laser ranging and mapping with a photon-counting detector, *Appl. Opt.*, **35**, 441–452.

Savigny, C., O. Funk, U. Platt, and K. Pfeilsticker, 1999: Radiative smoothing in zenith-scattered sky light transmitted through clouds to the ground, *Geophys. Res. Lett.*, **26**, 2949-2952.

Winker, D.M., R.H. Couch, and M.P. McCormick, 1996: An overview of LITE: NASA's Lidar In-space Technology Experiment, *Proc. IEEE*, **84**, 164–180.

Winker, D.M., 1997: Simulation and modeling of the multiple scattering effects observed in LITE data, *Advances in Atmospheric Remote Sensing with Lidar*, Eds. A. Ansmann et al., Springer-Verlag, pp. 185–188.